Interfacial antiferromagnetic coupling between $SrRuO_3$ and $La_{0.7}Sr_{0.3}MnO_3$ with orthogonal easy axis

Qing Qin,[1] Shikun He,[2] Weinan Lin,[1] Herng Yau Yoong,[1] Liang Liu,[1] Mengsha Li,[1] Stephen John Pennycook,[1] Wen Xiao,[1] Ping Yang,[3] Wendong Song,[2] and Jingsheng Chen[1,*]

[1]*Department of Materials Science and Engineering, National University of Singapore, Singapore 117575, Singapore*

[2]*Data Storage Institute, Agency for Science, Technology and Research (A*STAR), 2 Fusionopolis Way #08-01 Innovis, Singapore 138634*

[3]*Singapore Synchrotron Light Source (SSLS), National University of Singapore, 5 Research Link, Singapore 117603*

(Received 3 July 2018; revised manuscript received 12 September 2018; published 11 October 2018)

Engineering exchange interaction between magnetic thin films is a key ingredient for achieving high-performance spintronics devices. In this work, the exchange coupling effect of bilayers consisting of perpendicularly magnetized tetragonal phase $SrRuO_3$ (SRO) and in-plane magnetized $La_{0.7}Sr_{0.3}MnO_3$ has been investigated. We observed an intriguing antiferromagnetic exchange coupling at the interface of such heterostructures with orthogonal magnetic configuration. The unique exchange coupling coexists with the formation of domain walls in the SRO layer as inferred from the magnetometry and magnetotransport measurements, resulting in a positive exchange bias effect. The thickness and temperature dependence of the bias field further confirm the interfacial origin of the antiferromagnetic coupling effect.

DOI: 10.1103/PhysRevMaterials.2.104405

I. INTRODUCTION

Exchange interaction which is originated from the overlapping of electron wave functions is essential for understanding magnetism. The interaction of electrons within an atom leads to the famous Hund's rule, whereas the interatomic interaction results in spontaneous magnetization and bonding of a material [1]. In thin films and heterostructures, exchange interaction between adjacent magnetic layers plays an important role and is inevitable for various emerging applications such as exchange-spring magnets, spin valves, and magnetic tunneling junctions [2,3]. Particularly, the interlayer exchange coupling is tailored in various forms to improve the device performance and reliability. For example, oscillatory interlayer exchange coupling mediated by conduction electrons, known as the RKKY interaction, allows both the strength and sign of the coupling to be tuned by the thickness of the nonmagnetic spacer layer between two ferromagnetic layers for desired functionalities [4–6]. Next, the interaction between an antiferromagnetic layer and a ferromagnetic layer results in an exchange bias effect which is suitable for pinning the reference layer in spin valves [7,8]. Also, the exchange coupling of a bilayer consisting of a magnetically hard layer and a soft layer with orthogonal easy axis exhibits exchange-spring behavior, which is used for increasing the energy products in permanent magnets [9]. Note that all the above-mentioned interactions occur in metallic ferromagnets.

On the other hand, ferromagnetic oxides have attracted much attention due to their potential application in all oxide spintronics and rich physics caused by the coupling among charge, orbital, spin, and lattice degrees of freedom [10,11]. The superexchange and double exchange interaction of magnetic metal cations mediated by oxygen anions are responsible for the observed antiferromagnetic and ferromagnetic behaviors of the perovskite oxides. The exchange coupling of perovskite oxide bilayers such as $SrRuO_3/La_{0.7}Sr_{0.3}MnO_3$ (SRO/LSMO) was reported to be antiferromagnetic coupling, where the SRO layer exhibits a monoclinic phase with Ru moment in an orientation 30°–45° away from the c axis [12,13]. The origin of the antiferromagnetic coupling has been attributed to superexchange interaction between Mn and Ru ions; the moments of both ions have a nonzero projection in the film plane [14]. Until now, the investigation of exchange coupling between Mn and Ru ions with perpendicular magnetic moment is still lacking. The hosting material, such as magnetic bilayers with orthogonal easy axes can maximize the spin transfer torque (STT) when spin-polarized current is injected across the interface [15]. Hence this is promising for reducing the switching current density [16], increasing the write speed of magnetic random access memory [17,18], and improving the performance of spin-torque oscillators [19].

In this work, we study the interlayer exchange coupling between a tetragonal phase $SrRuO_3$ (T-SRO) layer with strong perpendicular uniaxial anisotropy and a $La_{0.7}Sr_{0.3}MnO_3$ (LSMO) layer with easy axis in the film plane; i.e., the easy axes of two adjacent magnetic layers are orthogonal to each other. Here, the magnetization reversal of the bilayers with fixed T-SRO thickness and varying LSMO thickness (t) were investigated. It was found that the antiferromagnetic coupling between SRO and LSMO at the interface are developed at temperatures lower than the Curie temperature (T_c) of SRO. Remarkably, we found that the coupling effect is closely related to the perpendicular stripe domain wall of the SRO layer. An exchange bias effect exerted on the LSMO layer was observed due to this interfacial phenomenon. We also studied the LSMO thickness and temperature dependent exchange

*Email address: msecj@nus.edu.sg

bias field, which demonstrates the potential application of this unique effect.

II. EXPERIMENTS

T-SRO (18 nm)/LSMO ($t = 2$, 4, 8, and 12 nm) bilayers were grown on (001) $SrTiO_3$ (STO) substrate by pulsed laser deposition (PLD) with a KrF excimer laser (248 nm, 2 Hz) and a laser fluence of 1.5–1.8 J/cm^{-2}. The distance between the substrate and the target was kept at 60 mm during the deposition. The growth temperatures are 750 °C and 900 °C for SRO and LSMO, respectively. During the deposition, the oxygen partial pressure was 20 and 200 mTorr for SRO and LSMO to form the desired phases. Subsequently, the samples were cooled to room temperature at a rate of 10 °C/min under 1 Torr oxygen partial pressure. The crystal structures were characterized by the high-resolution x-ray diffractometer using synchrotron x-ray sources. The magnetoresistance and angular dependent magnetoresistance were investigated by the linear array four-point probe method using the physical property measurement system (PPMS: Quantum Design). Temperature dependent magnetization and hysteresis loops were measured by a superconducting quantum interference device (SQUID).

III. RESULT AND DISCUSSION

The crystallographic structures of the bilayers were characterized by the x-ray diffraction (XRD) L scan of the reciprocal space. The XRD spectrum for the sample with $t = 12$ nm is shown in Fig. 1(b). Laue oscillations are clearly identified near the peaks corresponding to SRO and LSMO beside STO (00l), which indicates the good crystallinity of the layers. Reciprocal space mappings (RSMs) at {013} STO reflections were shown in Fig. 1(c). The bottom peaks are identified as SRO {013} reflections since the film is under a compressive strain, while the top peaks are from the LSMO layer which is under a tensile strain. The equal L values of the four different {013} reflections indicate that the lattice vector a/b is perpendicular to c. Therefore, both the SRO and LSMO layers possess the tetragonal phase.

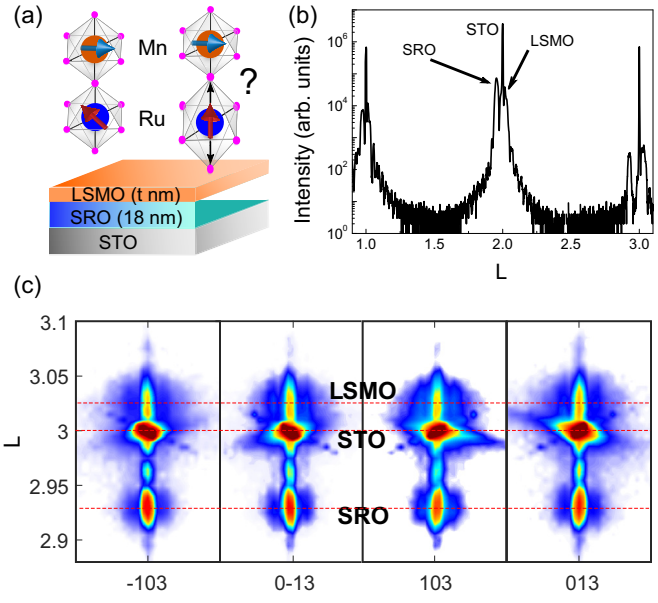

FIG. 1. Structure characterization. (a) Illustration of the SRO/LSMO bilayer structure deposited on STO. (b) Reciprocal L scan and (c) RSMs around {013} reflections of the bilayer with $t = 12$ nm.

The in-plane (IP) and out-of-plane (OP) hysteresis loops (MH) of the LSMO and SRO single layers are shown in Fig. 2(a) and 2(b), respectively. The results show that T-SRO has good perpendicular anisotropy, which is consistent with our previous report [20,21]. The saturation magnetization of T-SRO at 10 K is 210 emu/cc or 1.375 μ_B per Ru ion (Fig. 3 in the Supplemental Material [22]) indicating that Ru is in a low-spin configuration [23]. On the other hand, LSMO saturation magnetization at 10 K is 605 emu/cc or 3.81 μ_B per Mn ion (Fig. 2 in the Supplemental Material [22]). Figure 2(c) (in the main text) shows the normalized MH loops of the samples in an OP magnetic field measured at 10 K. All samples exhibited superposition of a sharp magnetization reversal in the high-magnetic-field region and a gradual change of magnetization under low magnetic field. The former sudden magnetization reversal at a field around 17 kOe corresponds to the flip of the magnetically harder SRO layer whereas the latter gradual change of magnetization is due to the magnetically soft LSMO layer rotating its magnetization gradually to its hard axis. The switching field of SRO in the SRO/LSMO bilayer structure is the same as that of a SRO single layer. This behavior is different from that in a metallic hard/soft bilayer structure where the switching field is reduced with increasing thickness of the soft magnetic layer. The hysteresis loops measured with IP magnetic fields are shown in Fig. 2(d). Magnetization reversal occurs at 1–2 kOe, which corresponds to the coercive fields of LSMO layers. The vertical center of the bilayers in this study is at zero, indicating that the net in-plane magnetization of the SRO layer at 10 K is essentially zero due to its perpendicular easy axis and large anisotropy. Note that the vertical center of the IP MH loops of a bilayer with monoclinic phase SRO (M-SRO) and LSMO is nonzero [12,13], and is shifted to the magnetization values of the uncompensated SRO because the easy axis of M-SRO varies with temperature and has an angle of $30^\circ < \beta < 45^\circ$ with respect to the [001] axis [24].

To rule out the possibility of a tilted easy axis of SRO in the bilayers, the magnetization of the bilayer was further investigated by field angle dependent magnetoresistance (MR) measurement, which is useful for determining the easy and hard axes of multilayers [20]. The current was applied parallel to the [100] axis to perform a four-probe resistance measurement. An external field of 40 kOe perpendicular to the current was applied. The field was first rotated clockwise and then anticlockwise in the (100) plane. Figure 3 shows the field angle (θ, measured with respect to [001]) dependent MR of the bilayers with different t. According to our previous study, hysteresis centered around the hard axes of magnetic phases should be observed in a $R(\theta)$ loop. The width of the hysteresis region, on the other hand, depends on the strength of anisotropy. With $t = 2$, $R(\theta)$ showed a symmetric hysteresis behavior with a period of 180°. The centers of the hysteresis are at $\theta = 90^\circ$ and 270°, which corresponds to the hard axis

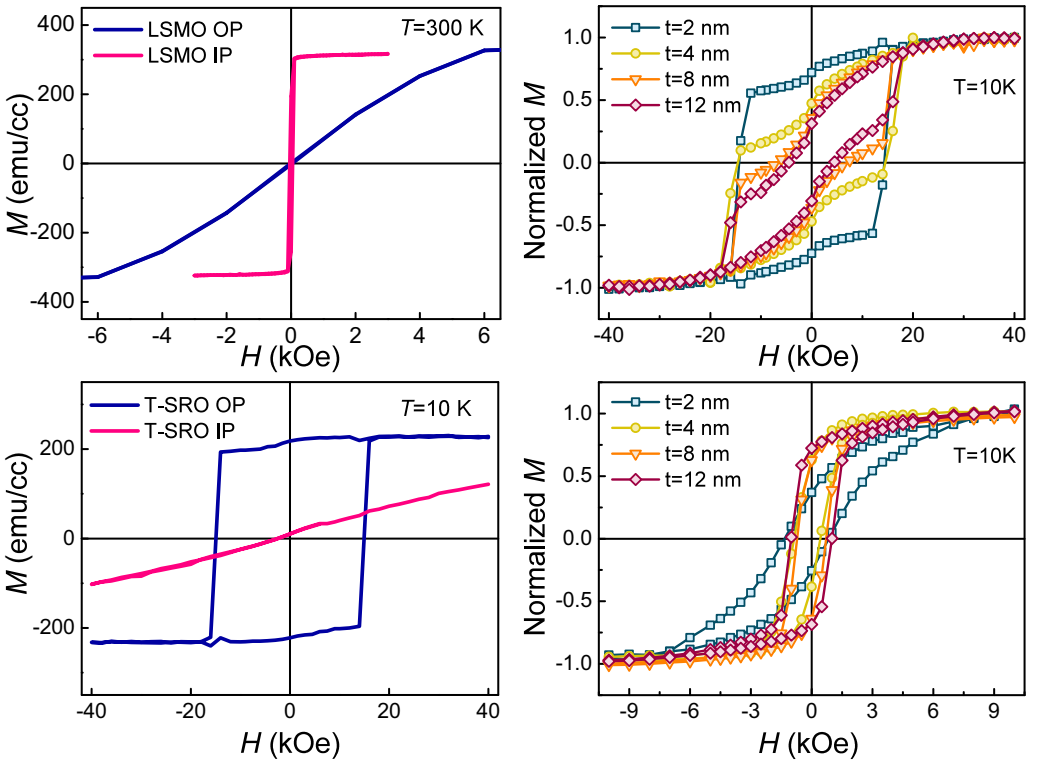

FIG. 2. Magnetic hysteresis loops of single-layer and bilayer samples. (a) In-plane and out-of-plane *M-H* loops of a 20-nm LSMO single-layer sample measured at 300 K. (b) In-plane and out-of-plane *M-H* loops of a 20-nm SRO single-layer sample measured at 10 K. (c) Out-of-plane and (d) in-plane *M-H* loops of SRO/LSMO bilayers with various LSMO thickness (t) measured at 10 K.

of T-SRO. Hence, the easy axis of SRO is perpendicular to the film plane. $R(\theta)$ curves of the bilayers with $t = 4$, 8, 12 nm, as shown in Figs. 3(b)–3(d), exhibited not only strong hysteresis at 90° and 270°, but also weak hysteresis at 180° and 360°. These weak hystereses are associated to the magnetization orientation jumps around the hard axis of LSMO. Thereby, the easy axis of LSMO is still in the film plane as a consequence of the demagnetization field.

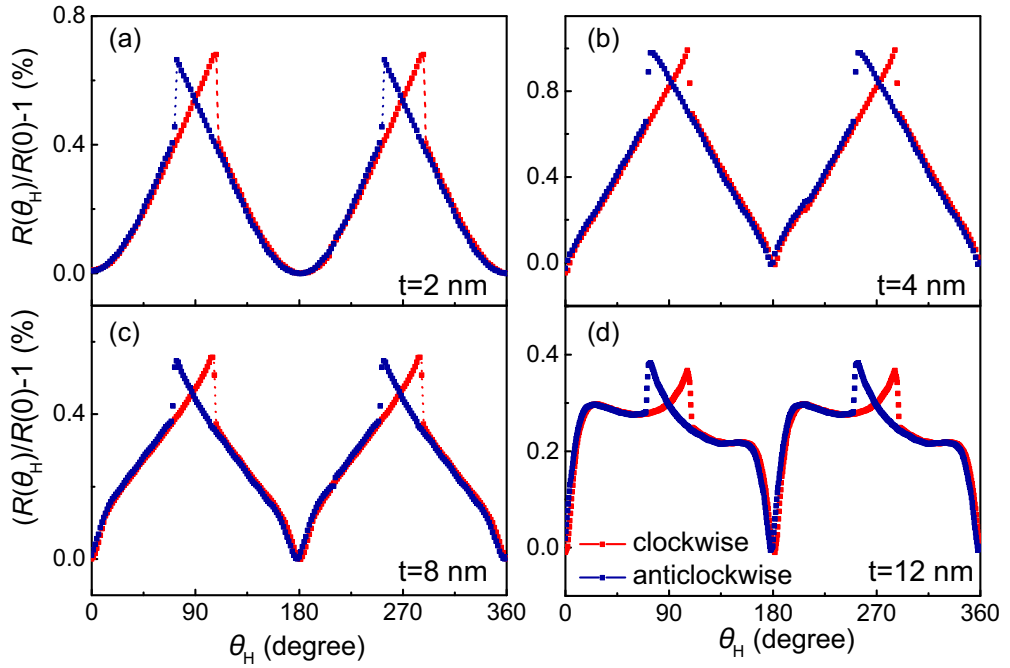

FIG. 3. Field angle dependent MR loops of SRO/LSMO bilayers at 10 K. (a–d) are the loops for $t = 2$, 4, 8, and 12 nm, respectively.

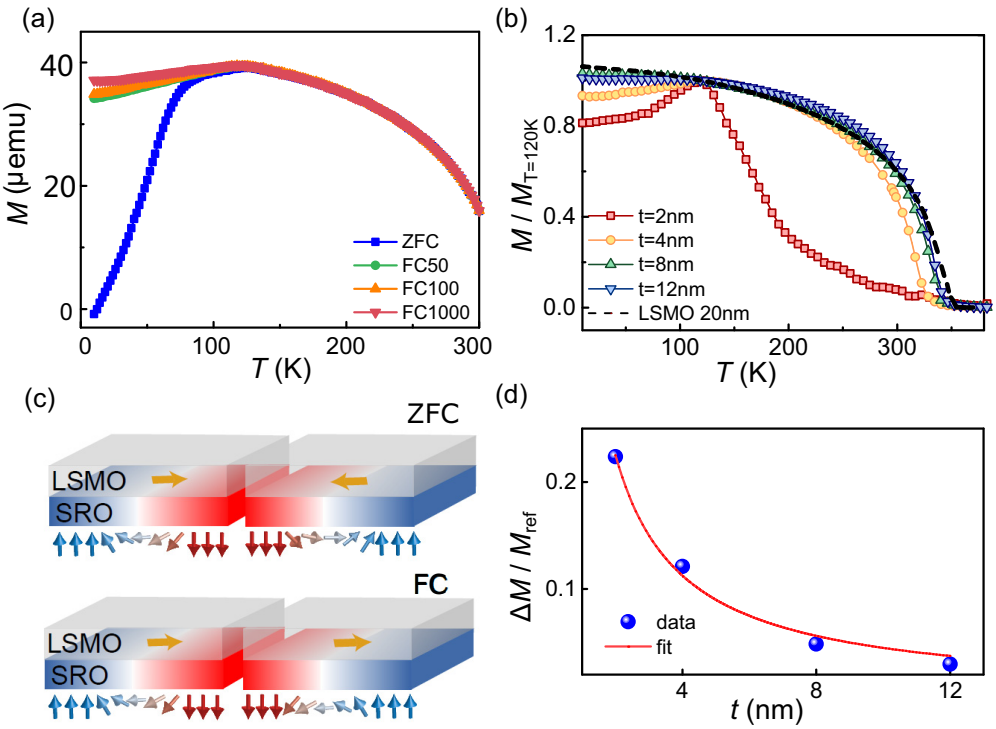

FIG. 4. Temperature dependent magnetization of the bilayers. (a) In-plane temperature dependence of magnetic moment of SRO/LSMO $t = 4$ nm bilayer. The sample was measured with a 1-kOe field after each cooling. The cooling fields are 0, 50, 100, and 1000 Oe (ZFC, FC50, FC100, and FC1000). (b) In-plane magnetization normalized by the moment at 120 K of the SRO/LSMO bilayers for various LSMO thicknesses measured with a 1-kOe field after field cooling at 1 kOe. The dashed line is the data taken from a 20-nm reference LSMO film. (c) Illustrations of the domain wall mediated AFM coupling between SRO and LSMO at different sample locations for ZFC and FC. (d) The compensated moment normalized by the moment of the reference sample at 10 K as a function of t. The compensated moment is defined as $\Delta M = M - M_{\text{ref}}$.

The temperature dependence of magnetization under different cooling conditions for the bilayer with $t = 4$ nm is shown in Fig. 4(a). The zero field cooling moment at low temperature decreases significantly due to the formation of domains in the LSMO. The formation of domain structures in LSMO grown on STO (under a tensile stress) have been verified by previous works [25–27] and the spins within the domains of very thin LSMO lie in the plane. For nonzero IP field cooling, a small drop in the moment is observed at $T <$ 120 K. Based on this observation and the MR measurement in Fig. 3, the magnetic configuration in this work hence is different from the M-SRO/LSMO bilayer studied previously [13] (see Figs. 2 and 5 in the Supplemental Material [22]). Particularly, in the M-SRO/LSMO bilayer, a transition from antiparallel to parallel alignment state between LSMO and SRO orientation by increasing cooling field is observed; therefore the magnetic moment can increase at lower temperature if a relative high cooling field is applied [13]. However, in our work, this phenomenon was not observed even for a cooling field as high as 40 kOe (see Fig. 4 in the Supplemental Material [22]) because of the orthogonal easy axis in T-SRO/LSMO structures. The temperature dependences of the IP magnetic moment of the bilayers measured with 1 kOe cooling field for different LSMO thicknesses are shown in Fig. 4(b). The Curie temperature (T_c) of the LSMO in the bilayer is thickness dependent. T_c for $t = 2$ nm is significantly lower than that of the thicker ones and the transition is much broader. More importantly, the magnetization of the bilayer showed very different temperature dependent behavior as compared to a LSMO single layer. As shown in the figure, the magnetization of a 20-nm LSMO single layer (reference) increases monotonically with decreasing temperature. However, in the bilayer structure, a significant drop in the IP moment at $T <$ 120 K is evident. Moreover, such moment reduction is even more obvious for the bilayer with a thinner LSMO layer. At $T = 10$ K, the perpendicular magnetic anisotropy for SRO is so strong that a measurement field of 1 kOe will have a negligible effect on SRO. Hence, the measured IP magnetization is mostly from the LSMO layer. Therefore, the drop in the normalized moment of the bilayer structures indicates that the bilayer loses some net IP magnetization at the T-SRO/LSMO interface. The observation is reminiscent of the phenomena reported in M-SRO/LSMO bilayers [13] and SRO/LSMO superlattices [28]. Ru in SRO and Mn from LSMO are responsible for the ferromagnetic order of individual layers. At the interface, Ru and Mn are separated by either a SrO or (La,Sr)O layer. First-principles calculations have shown that the hybridization of interfacial O $2p$ with Mn $3d$ states and Ru $4d$ states may result in antiparallel alignment of Mn and Ru atoms to achieve a lower-energy state [14].

However, the antiferromagnetic (AFM) coupling mechanism requires an in-plane component of the interfacial SRO magnetic moment. This is straightforward for M-SRO but is not expected for T-SRO. Two possible origins are deduced

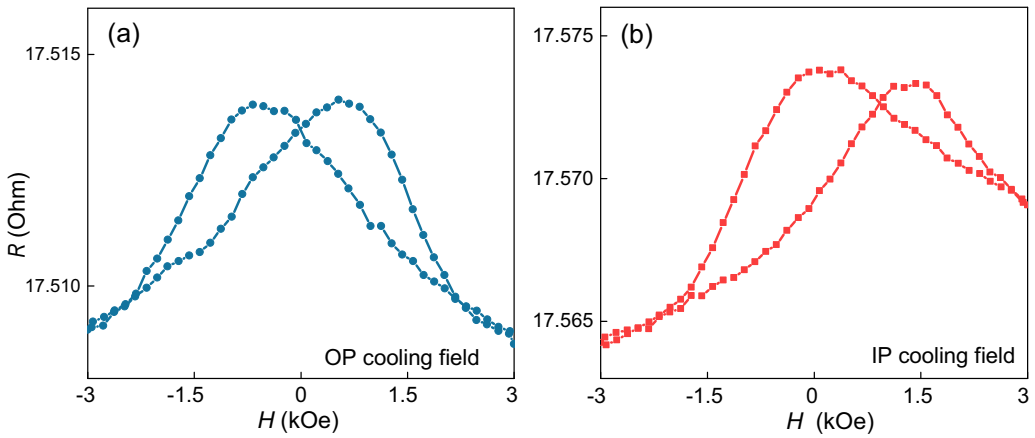

FIG. 5. IP MR hysteresis loops of the bilayers with different cooling field directions. (a) A 40 kOe field cooling from 370 to 10 K under OP field. (b) A 40 kOe field cooling from 370 to 10 K along the IP direction. The MR loops were measured at 10 K for a $t = 4$ nm sample.

to be responsible for the IP moment of T-SRO at the T-SRO/LSMO interface. In the first case, the interfacial layer of SRO behaves differently as compared to the bulk, and its magnetic easy axis is no longer in the perpendicular direction but slightly tilted similar to the M-SRO. A common origin of such property change is the interfacial mixing [28]. However, the mixing at the LSMO/SRO interface in our samples is negligibly small as shown by the scanning transmission electron microscopy results (see Fig. 1 in the Supplemental Material [22]). The second possible origin is related to the domain formation of SRO. When cooling the bilayer in a moderate in-plane field, the Zeeman energy of the SRO layer is much smaller than the anisotropy energy. Therefore, stripe pattern perpendicular domains will be formed. As a result, spin orientations in the domain walls separating individual domain regions vary spatially from up to down. Therefore an in-plane component of the SRO moment can exist in the domain walls. At zero cooling field, the orientations of such in-plane moments in the wall regions are distributed randomly [29–31] as illustrated in Fig. 4(c); the statistical average of the IP component of the magnetization is zero. Under a cooling field, the spin orientations of the domain walls tend to align with the field due to the associated Zeeman energy. Hence, net IP moments of interfacial SRO are developed. These moments are then exchange coupled to the LSMO layer through AFM coupling as illustrated in Fig. 4(c).

We assume that the moment of an interfacial LSMO layer with an effective thickness (d) is compensated by the SRO moment as a result of the AFM coupling at 10 K. In a rough estimation, d is independent of LSMO thickness $\frac{\Delta M}{M_{\rm ref}} = \frac{M_{\rm ref}-M}{M_{\rm ref}} = d/t$. The calculated values are shown in Fig. 4(d). The data are fitted well using $d = 0.45$ nm, indicating that the effective thickness of the compensated LMSO is slightly larger than one unit cell.

To confirm our assumption of domain wall assisted interfacial antiferromagnetic coupling, we measured the MR loop with different cooling field directions, hence magnetization configurations of SRO. In the first measurement, the sample was cooled down to 10 K with an OP field of 40 kOe to form a single-domain SRO. Subsequently, the OP field was removed and then IP fields smaller than the coercive field of SRO were applied to measure the MR loop. As can be seen in Fig. 5(a), the MR loop is symmetrical, indicating the absence of bias effect. In the second measurement, we cool the sample in an IP field of 40 kOe which is much lower than the saturation field of SRO on its hard axis, the MR loop is asymmetric and a large positive bias effect is observed as shown in Fig. 5(b). Hence, the formation of domain wall in the second measurement plays an important role for the bias effect and the underlying antiferromagnetic coupling at the interface.

Furthermore, the interfacial AFM exchange coupling also results in an exchange bias effect. In-plane minor loops of the bilayers are shown in Figs. 6(a)–6(d). In such experiments, samples were first cooled in an in-plane magnetic field of 40 kOe to 10 K. Hysteresis loops were then measured by sweeping the field between 3 and -3 kOe. It is found that the magnetization loops are shifted along the field axis in the same direction as the cooling field. These shifts of the M-H loops are direct evidence of positive exchange bias of the bilayers. The exchange fields $H_{\rm ex}$ determined are shown in Fig. 6(e). $H_{\rm ex}$ decreases with LSMO thickness, confirming its interfacial origin. The uniaxial anisotropy of T-SRO is about 1.2×10^6 J/m^3. Therefore, the domain wall width at 10 K is about 4.1 nm determined by the following relation: $w = \pi\sqrt{A/K}$. Here, $A = 2$ pJ/m is the exchange stiffness [32]. On the other hand, the typical domain spacing (S) of perpendicularly magnetized SRO revealed by Lorentz microscopy is about 200 nm [30]. The spacing between the stripe domains depends on both the saturation magnetization and the wall energy (γ): $S = \sqrt{\gamma t/1.7M_s^2}$ [30]. Theoretically, the domain could increase with decreasing temperature due to the rapid change of the anisotropy energy with temperature. However in reality, the actual domain size will not change much in a cooling process because the annihilation of walls requires additional energy to move the existing domain walls. Therefore, it is reasonable to use 200 nm as the typical domain spacing to calculate the bias field. When the external field is equal to the exchange bias field, the Zeeman energy is compensated by the interfacial exchange interaction energy. Hence, the bias field $H_{\rm ex}$ can be estimated using $H_{\rm ex} = \frac{J_{\rm AF}}{M_s t}(w/S)$. Here, the factor w/S accounts for the fact that the domain wall mediated

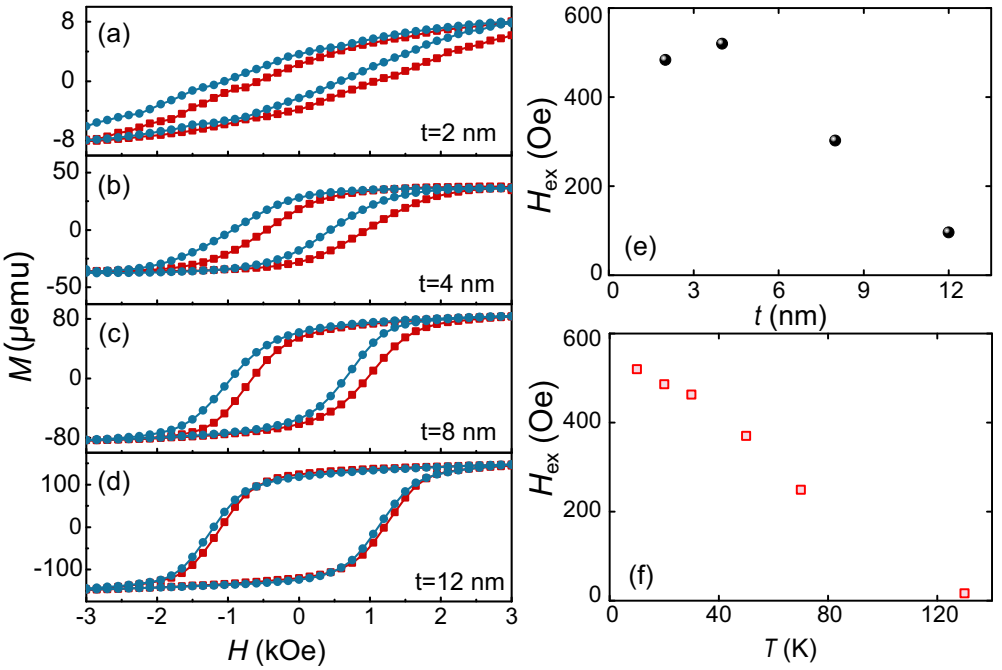

FIG. 6. Exchange bias effect. (a–d): In-plane hysteresis loops of the SRO/LSMO bilayers with positive cooling field (square) and negative cooling field (circle) for different LSMO thicknesses. (e) Exchange bias field as a function of LSMO thickness. (f) Temperature dependence of the exchange bias field for a $t = 4$ nm sample.

exchange coupling is only exerted locally on the LSMO films on top of the SRO domain walls. Using $J_{AF} = -320\,\mu J/m^2$ reported by Solignac *et al.* [33], H_{ex} for the bilayer with a 4-nm-thick LSMO at low temperature is estimated to be 82 Oe. This calculated exchange field is several times lower than the observed value of 500 Oe. Although the discrepancy seems large, the exchange bias effect coupled by perpendicular stripe domain walls is favored considering that an exchange bias field of more than 1 T is expected for fully in-plane magnetized SRO and LSMO [32].

It is worth noting that the interfacial exchange interaction between two ferromagnetic layers tends to be ferromagnetic as indicated by a negative exchange bias field [20]. However, positive exchange bias due to the formation of magnetic domain walls has also been observed in systems with an antiferromagnet or ferrimagnet bias layer [34,35]. For example, the exchange bias effect originating from antiferromagnetic coupling between Mn and induced moment in $BiFeO_3$ at the interface was reported in a LSMO/$BiFeO_3$ bilayer [36]. For our T-SRO/LSMO structure, we attribute the observed exchange bias to the antiferromagnetic coupling between Mn and Ru similar to the M-SRO/LSMO bilayer [37]. To confirm the speculation, *M-H* loops under different temperatures were measured. Figure 6(f) shows the temperature dependence of the exchange bias field. H_{ex} decreases with temperature and drops to zero near the Curie temperature of SRO. Thereby, the exchange bias effect is correlated to the magnetic order of SRO through the establishment of antiferromagnetic alignment of spins at the T-SRO/LSMO interface.

IV. CONCLUSION

In summary, the magnetic coupling of tetragonal phase SRO and LSMO bilayers was investigated, where the SRO and LSMO layers exhibited out-of-plane and in-plane easy axis, respectively. At the interface, an antiferromagnetic coupling between Ru and Mn atoms was unexpectedly observed. Possible phenomenological origin of the coupling including the formation of the SRO domain wall is discussed. The exchange coupling results in a positive exchange bias effect on LSMO. The effective thickness of LSMO where the magnetic moment is being compensated at the interface is slightly more than one atomic layer. The interfacial origin and the correlation to the ferromagnetic SRO of the exchange bias were confirmed by the LSMO thickness and temperature dependence of the bias field.

ACKNOWLEDGMENTS

The research is supported by the Singapore National Research Foundation under CRP Award No. NRF-CRP10-2012-02 and IIP Award No. NRF-IIP001-001. P.Y. is supported from SSLS via NUS Core Support No. C-380-003-003-001.

Q.Q. and S.H. contributed equally to this work.

[1] J. Stöhr and H. C. Siegmann, *Magnetism: From Fundamentals to Nanoscale Dynamics* (Springer, Berlin, Heidelberg, 2006).

[2] D. C. Ralph and M. D. Stiles, J. Magn. Magn. Mater. **320**, 1190 (2008).

[3] S. Ikeda, K. Miura, H. Yamamoto, K. Mizunuma, H. D. Gan, M. Endo, S. Kanai, J. Hayakawa, F. Matsukura, and H. Ohno, Nat. Mater. **9**, 721 (2010).

[4] S. S. P. Parkin, N. More, and K. P. Roche, Phys. Rev. Lett. **64**, 2304 (1990).

[5] A. Fert, A. Barthélémy, P. Galtier, P. Holody, R. Loloee, R. Morel, F. Pétroff, P. Schroeder, L. B. Steren, and T. Valet, Mater. Sci. Eng. B **31**, 1 (1995).

[6] K. Yakushiji, A. Sugihara, A. Fukushima, H. Kubota, and S. Yuasa, Appl. Phys. Lett. **110**, 092406 (2017).

[7] J. Nogues and I. K. Schuller, J. Magn. Magn. Mater. **192**, 203 (1999).

[8] N. H. March, P. Lambin, and F. Herman, J. Magn. Magn. Mater. **44**, 1 (1984).

[9] L. S. Huang, J. F. Hu, and J. S. Chen, J. Magn. Magn. Mater. **324**, 1242 (2012).

[10] M. Bibes, J. E. Villegas, and A. Barthélèmy, Adv. Phys. **60**, 5 (2011).

[11] A. Bhattacharya and S. J. May, Annu. Rev. Mater. Res. **44**, 65 (2014).

[12] X. Ke, M. S. Rzchowski, L. J. Belenky, and C. B. Eom, Appl. Phys. Lett. **84**, 5458 (2004).

[13] X. Ke, L. J. Belenky, V. Lauter, H. Ambaye, C. W. Bark, C. B. Eom, and M. S. Rzchowski, Phys. Rev. Lett. **110**, 237201 (2013).

[14] Y. Lee, B. Caes, and B. N. Harmon, J. Alloys Compd. **450**, 1 (2008).

[15] J. C. Slonczewski, J. Magn. Magn. Mater. **159**, L1 (1996).

[16] R. Law, E.-L. Tan, R. Sbiaa, T. Liew, and T. C. Chong, Appl. Phys. Lett. **94**, 062516 (2009).

[17] M. Marins de Castro, R. C. Sousa, S. Bandiera, C. Ducruet, A. Chavent, S. Auffret, C. Papusoi, I. L. Prejbeanu, C. Portemont, L. Vila, U. Ebels, B. Rodmacq, and B. Dieny, J. Appl. Phys. **111**, 07C912 (2012).

[18] H. Liu, D. Bedau, D. Backes, J. A. Katine, J. Langer, and A. D. Kent, Appl. Phys. Lett. **97**, 242510 (2010).

[19] D. Houssameddine, U. Ebels, B. Delaet, B. Rodmacq, I. Firastrau, F. Ponthenier, M. Brunet, C. Thirion, J. P. Michel, L. Prejbeanu-Buda, M. C. Cyrille, O. Redon, and B. Dieny, Nat. Mater. **6**, 447 (2007).

[20] Q. Qin, W. Song, S. He, P. Yang, and J. Chen, J. Phys. D: Appl. Phys. **50**, 215002 (2017).

[21] W. Lu, P. Yang, W. D. Song, G. M. Chow, and J. S. Chen, Phys. Rev. B **88**, 214115 (2013).

[22] See Supplemental Material at http://link.aps.org/supplemental/10.1103/PhysRevMaterials.2.104405 for scanning transmission electron microscopy image and more magnetization data.

[23] A. J. Grutter, F. J. Wong, E. Arenholz, A. Vailionis, and Y. Suzuki, Phys. Rev. B **85**, 134429 (2012).

[24] L. Klein, J. S. Dodge, C. H. Ahn, G. J. Snyder, T. H. Geballe, M. R. Beasley, and A. Kapitulnik, Phys. Rev. Lett. **77**, 2774 (1996).

[25] C. Kwon, M. C. Robson, K.-C. Kim, J. Y. Gu, S. E. Lofland, S. M. Bhagat, Z. Trajanovic, M. Rajeswari, T. Venkatesan, A. R. Kratz *et al.*, J. Magn. Magn. Mater. **172**, 229 (1997).

[26] J. Dho and N. H. Hur, J. Magn. Magn. Mater. **318**, 23 (2007).

[27] S. R. Bakaul, W. Lin, and T. Wu, Appl. Phys. Lett. **99**, 42503 (2011).

[28] M. Ziese, I. Vrejoiu, E. Pippel, P. Esquinazi, D. Hesse, C. Etz, J. Henk, A. Ernst, I. V. Maznichenko, W. Hergert, and I. Mertig, Phys. Rev. Lett. **104**, 167203 (2010).

[29] L. Klein, A. F. Marshall, J. W. Reiner, C. H. Ahn, T. H. Geballe, M. R. Beasley, and A. Kapitulnik, J. Magn. Magn. Mater. **188**, 319 (1998).

[30] A. F. Marshall, L. Klein, J. S. Dodge, C. H. Ahn, J. W. Reiner, L. Mieville, L. Antagonazza, A. Kapitulnik, T. H. Geballe, and M. R. Beasley, J. Appl. Phys. **85**, 4131 (1999).

[31] L. Klein, Y. Kats, A. F. Marshall, J. W. Reiner, T. H. Geballe, M. R. Beasley, and A. Kapitulnik, Phys. Rev. Lett. **84**, 6090 (2000).

[32] M. Ziese, I. Vrejoiu, and D. Hesse, Appl. Phys. Lett. **97**, 052504 (2010).

[33] A. Solignac, R. Guerrero, P. Gogol, T. Maroutian, F. Ott, L. Largeau, P. Lecoeur, and M. Pannetier-Lecoeur, Phys. Rev. Lett. **109**, 027201 (2012).

[34] S. Mangin, F. Montaigne, and A. Schuhl, Phys. Rev. B **68**, 140404 (2003).

[35] J. Nogués, D. Lederman, T. J. Moran, and I. K. Schuller, Phys. Rev. Lett. **76**, 4624 (1996).

[36] P. Yu, J.-S. Lee, S. Okamoto, M. D. Rossell, M. Huijben, C.-H. Yang, Q. He, J. X. Zhang, S. Y. Yang, M. J. Lee, Q. M. Ramasse, R. Erni, Y.-H. Chu, D. A. Arena, C.-C. Kao, L. W. Martin, and R. Ramesh, Phys. Rev. Lett. **105**, 027201 (2010).

[37] X. K. Ning, Z. J. Wang, X. G. Zhao, C. W. Shih, and Z. D. Zhang, J. Appl. Phys. **113**, 223903 (2013).